Does Tetrahydrofuran Ring Open upon Ionization and Dissociation? A TPES and TPEPICO Investigation

Paul M. Mayer,*,† Martyn F. Guest,‡ Louise Cooper,§ Larisa G. Shpinkova,‖ Emma E. Rennie,†,# David M. P. Holland,⊥ and David A. Shaw⊥

Department of Chemistry, University of Ottawa, 10 Marie-Curie, Ottawa, Canada K1N 6N5, Advanced Research Computing, Cardiff University, Redwood Building, King Edward VII Avenue, Cardiff CF10 3NB Wales, U.K., Department of Chemistry, Heriot-Watt University, Riccarton, Edinburgh EH14 4AS, U.K., Department of Nuclear Spectroscopy Methods, Institute of Nuclear Physics, Moscow State University, Moscow 119899, Russia, and Daresbury Laboratory, Daresbury, Warrington, Cheshire WA4 4AD, U.K.

Received: July 8, 2009; Revised Manuscript Received: September 1, 2009

The threshold photoelectron spectrum (TPES) of tetrahydrofuran (THF) is compared to that of the unsaturated furan molecule. In general, there is a similarity in the orbital ionization profile for the two species, though unlike furan, THF exhibits (modest) vibrational detail only in the $(9b)^{-1}$ $\tilde{X}$ ^2B band. An adiabatic ionization energy of 9.445 ± 0.010 eV has been derived from the onset of the TPES spectrum. Threshold photoelectron photoion coincidence spectroscopy was used to explore the loss of a hydrogen atom from ionized THF over the photon energy range of 9.9−10.4 eV. RRKM fitting of the resulting breakdown curves yields an E_0 of 0.85 ± 0.03 eV (82 ± 3 kJ mol^{-1}) (AE = 10.30 ± 0.04 eV). If the G3 IE of 9.48 eV is used to convert the experimental data from photon energy to THF ion internal energy, E_0 = 0.81 ± 0.01 eV (78 ± 1 kJ mol^{-1}). The latter value is closer to the G3 E_0 of 72 kJ mol^{-1} for the formation of the cyclic ion **1**. A variety of ring-opening reactions were also probed at the B3-LYP/6-31+G(d) and G3 levels of theory. The distonic isomer $^{\bullet}CH_2CH_2CH_2OCH_2^+$ lies 70 kJ mol^{-1} higher than ionized THF, which places it within 1 kJ mol^{-1} of the threshold for the dissociation to **1**. All of the probed H-loss products from the distonic isomer (which includes singlet and triplet species) lie significantly higher in energy than ion **1**, eliminating the possibility that ionized THF dissociates to *m*/*z* 71 via a ring-opening reaction in the present experiment. The derived $\Delta^{\ddagger}S$ value for the dissociation, 8 ± 5 J K^{-1} mol^{-1}, is also consistent with the formation of **1**. The experimentally derived E_0 values can be used to derive the $\Delta_f H^o_0$ for ion **1**. Together with the $\Delta_f H^o_0$ values for the THF ion (752.0 ± 2 kJ mol^{-1}, derived from the neutral $\Delta_f H^o_0$ of −154.9 ± 0.7 kJ mol^{-1} and experimental IE of 9.445 ± 0.010 eV) and H atom (218.5 kJ mol^{-1}) our E_0 of 82 ± 3 kJ mol^{-1} yields a $\Delta_f H^o_0$ for ion **1** of 620 ± 4 kJ mol^{-1} ($\Delta_f H^o_{298}$ = 594 ± 4 kJ mol^{-1}), in good agreement with the G3 $\Delta_f H^o_0$ of 621 kJ mol^{-1}. Appearance energies for all fragment ions up to photon energies of 34 eV are also reported and discussed in comparison with the available literature.

Introduction

There has been significant interest shown in the identification and chemistry of ions with composition $C_4H_7O^+$, *m*/*z* 71.[1−13] While an extensive review of the area is outside the scope of this paper, briefly, the members of this family of even electron gas-phase ions can be classified according to their analogous molecular structures (formed by H-atom addition): alcohols,[6,10,11] linear[2,4,5,7−9] and cyclic[1−3,10,13] ethers, aldehydes,[1,6] and ketones.[1,6] An observation common to all mass spectrometry-based investigations is that ionized tetrahydrofuran (THF) dissociates primarily by loss of a hydrogen atom. The structure usually assigned to the resulting fragment ion is the cyclic ether product **1**:

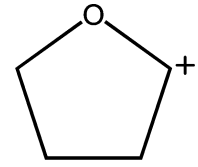

1

The evidence provided to support this assignment is that methyltetrahydrofuran ions lose a methyl group to form a product ion with *m*/*z* 71 having a collision-induced dissociation (CID) mass spectrum identical to that made by H-atom loss from tetrahydrofuran ions. However, it is apparent in the literature that the situation may not be so simple. As early as 1975 Krenmayr[1] showed from high resolution mass spectrometry studies that metastable *m*/*z* 71 ions originating by H loss from THF lose CO (and not C_2H_4, which has also been confirmed by d-labeling studies),[3] and he proposed that the $C_4H_7O^+$ ion ring-opened prior to the reaction. One possibility that arises from these observations is that the precursor THF ion ring-opens prior to H-atom loss to form a distinct, noncyclic fragment ion with

* Corresponding author. E-mail: pmmayer@uottawa.ca. Fax: (613) 562-5170.
† University of Ottawa.
‡ Cardiff University.
§ Heriot-Watt University.
‖ Moscow State University.
⊥ Daresbury Laboratory.
Present address: Varian, Inc., 2700 Mitchell Drive, Walnut Creek, CA 94598.

10.1021/jp906440p CCC: $40.75
Published on Web 09/23/2009

m/*z* 71. A more recent collision cross-section study by van Houte and van Thuijl[13] appears to support this hypothesis. While the collision cross-section of ionized THF was found to be largely consistent with a cyclic structure, allowance was made for the participation of a ring-opened distonic ion isomer, $^{\bullet}CH_2CH_2CH_2OCH_2^+$. In addition, the cross-section measurements on the *m*/*z* 71 product ion were consistent with a noncyclic species. So, it appears that there is some uncertainty about the nature of the dissociation reaction involving H-atom loss from ionized THF. To explore this further, we have performed threshold photoelectron spectroscopy (TPES) on neutral THF and threshold photoelectron-photoion coincidence spectroscopy (TPEPICO) to obtain quantitative information on the energetic and entropic properties of the dissociation.

Experimental Procedure

The pulsed TPEPICO spectrometer,[14] in which the dissociation, kinetic, and threshold photoelectron studies were performed, and the 5 m normal incidence monochromator,[15] attached to the Daresbury Laboratory synchrotron radiation source, have been described in detail previously. Briefly, the coincidence spectrometer employs a pulsed extraction technique,[16] the principal advantage of which is that threshold electrons can be detected with a high energy resolution, while also allowing the associated ions to be collected with a high mass resolution. In the present arrangement,[14] a very low electric field is applied initially across the interaction region to extract threshold electrons, the detection of which triggers the application of a high voltage (~1 kV) pulse across the region to draw the ion toward the drift tube, initiating the time-of-flight (TOF) measurement. The time between the arrival of the electron and the associated ion is measured electronically, with the summation of many events producing a TOF spectrum. By varying the delay between the detection of the threshold electron and the application of the ion extraction pulse, we can measure breakdown curves as a function of ion residence time in the interaction region. With the present apparatus the minimum residence time has been measured as 1.116 ± 0.050 μs, using the experimental procedure described in Holland et al.[14] The breakdown curves in the dissociation threshold energy region were measured for three residence times by adding additional electronic delays of 2 μs. That is, the actual residence times were 1.116, 3.116, and 5.116 μs. A complete breakdown curve between photon energies of 9.9 to 34 eV was acquired at the 1.116 μs residence time.

The threshold photoelectron spectrum was recorded in the binding energy range from 9.9 to 30 eV using only the electron detection part of the coincidence spectrometer. This consists of a lens optimized for high transmission of low energy electrons followed by a 100 mm mean radius hemispherical electrostatic analyzer. The lens accelerates the electrons to the chosen (typically 10 eV) analyzer pass energy, and the chromatic aberrations are such that only electrons having initially zero energy are brought to a focus at the analyzer entrance aperture. The spectrum was normalized to the incident photon intensity using the signal from a photomultiplier monitoring the radiation after it impinged upon a sodium salicylate coated screen. The threshold photoelectron spectrum was measured at a photon resolution of 0.1 nm fwhm (~18 meV at $h\nu = 15$ eV). Lithium fluoride or indium filters could be inserted into the photon beam exiting the monochromator to help suppress higher order radiation. The binding energy scale was calibrated by recording a threshold photoelectron spectrum of a gas mixture comprising THF, argon, and xenon.

Computational Procedures

Standard ab initio molecular orbital calculations[17] were performed using the Gaussian 98[18] suite of programs. Geometries for the ionic and neutral species were optimized and harmonic vibrational frequencies were calculated at the B3-LYP/6-31+G(d) level of theory. The resulting geometries and zero-point energies (ZPEs) (scaled by 0.98)[19] were then used to obtain G3[20] total energies. In our thermochemical estimations, the recommended $\Delta_f H$ values tabulated in the NIST Chemistry Database[21] and by Lias et al.[22] have been used unless stated otherwise. The G3 total energies were translated to enthalpies of formation according to the atomization procedure described by Nicolaides et al.[23] Thermal corrections to literature thermochemical values reported at 298 K were performed with the calculated harmonic frequencies where required.

Vertical ionization energies and their relative spectral intensities (pole strengths) of THF and furan were obtained using the outer valence Green's function (OVGF) approach.[24] The calculations employed the GAMESS-UK[25,26] suite of programs, with a variety of basis sets. For consistency, the geometries of both species were fully optimized at the MP2 level using both cc-pVTZ and cc-pVDZ basis sets.[27−30] The OVGF calculations were performed at the cc-pVTZ optimized equilibrium geometries of C_2 symmetry for THF and C_{2v} symmetry for furan using the cc-pVDZ basis set. Five inner shell orbitals—the 1s functions on each C and O—were frozen. The results are listed in Tables 1 and 2, together with charge distribution analyses derived from a Mulliken population analysis of the single configuration—the Hartree−Fock SCF wave function—generated at the same geometry used in the OVGF calculations.

The lowest energy dissociation channels were modeled with the standard RRKM rate expression:

$$k(E) = \frac{\sigma}{h} \frac{N^{\ddagger}(E - E_0)}{\rho(E)} \qquad (1)$$

where $k(E)$ is the unimolecular rate constant at an ion internal energy, E, σ is the reaction degeneracy or symmetry number, h is Planck's constant, E_0 is the 0 K activation energy, $\rho(E)$ is the reactant ion ro-vibrational density of states, and $N^{\ddagger}(E-E_0)$ is the transition state ro-vibrational sum of states.[31,32] The density and sum of states calculations employed the direct count algorithm of Beyer and Swinehart.[33] The ion frequencies were taken from the B3-LYP/6-31+G(d) geometry. The $k(E)$ was then convoluted with the parent ion thermal (rotational and vibrational) energy, the monochromator band-pass function (photon resolution ~8 meV), and the threshold electron analyzer transmission function (width of ~9 meV full width at half-maximium) derived from a threshold electron spectrum obtained from the photoionization of krypton in the region of the $^2P_{1/2}$ ionization limit under the conditions used in the TPEPICO measurements.[34−36] The activation energy, E_0, and the transition states vibrational frequencies (reflected in the activation entropy, $\Delta^{\ddagger}S$) were varied in the RRKM calculation until a satisfactory fit to the experimental breakdown curves, obtained at ion residence times of 1.116, 3.116, and 5.116 μs, was found. The necessity to fit all three breakdown diagrams simultaneously greatly reduces the range of E_0 and $\Delta^{\ddagger}S$ that gave satisfactory fits to the data.[37] The uncertainties quoted in the Results and Discussion reflect the deviation in these two parameters across all of the acceptable fits.

TABLE 1: Experimental and OVGF Vertical Ionization Energies and Charge Distribution Analyses of THF

				orbital character (% atomic population)							
	ionization energy (eV)			oxygen			carbon			hydrogen	
orbital	OVGF	experiment	pole strength OVGF	s	p	d	s	p	d	s	p
4a				68.4	2.0	0.0	18.8	8.0	1.5	1.3	0.0
5a				7.8	0.7	0.0	69.0	9.5	1.2	11.2	0.5
3b	24.13	23.3	0.86	0.0	9.3	0.3	65.9	5.4	0.8	17.6	0.8
4b	20.05	19.6	0.88	0.0	10.1	0.1	38.1	21.1	0.9	28.6	1.0
6a	19.98	19.6	0.89	5.5	1.9	0.0	40.5	21.1	1.0	28.7	1.3
5b	17.07	16.60	0.90	0.0	18.9	0.1	0.4	50.9	0.4	28.4	0.9
7a	16.70	16.60	0.90	2.3	20.5	0.3	1.3	52.0	1.2	21.6	0.8
8a	15.02	15.24	0.91	0.0	0.0	0.2	0.0	57.6	1.1	40.1	1.0
6b	14.86	14.41	0.90	0.0	34.0	0.2	1.5	41.7	1.7	20.2	0.7
7b	14.23	13.99	0.91	0.0	26.1	0.3	1.6	40.2	2.7	28.5	0.7
9a	12.63	12.84	0.91	0.8	25.0	0.0	0.4	49.4	2.3	21.3	0.8
8b	12.43	12.59	0.91	0.0	0.1	0.1	0.7	69.3	2.8	25.7	1.2
10a	12.24	11.96	0.92	0.1	1.2	0.1	0.0	48.8	3.7	45.4	0.6
11a	11.57	11.41	0.91	2.2	27.2	0.0	0.2	61.3	2.1	5.6	1.4
9b	9.88	9.76	0.91	0.0	53.7	0.0	0.0	13.9	3.2	29.1	0.1

TABLE 2: Experimental and OVGF Vertical Ionization Energies and Charge Distribution Analyses of Furan

			orbital character (% atomic population)							
	ionizationenergy(eV)		oxygen			carbon			hydrogen	
orbital	OVGF	experiment	s	p	d	s	p	d	s	p
$4a_1$			66.4	2.4	0.1	20.3	8.9	2.0	0.0	0.0
$5a_1$			8.5	1.5	0.0	72.7	14.3	1.5	1.8	0.0
$3b_2$			0.0	16.0	0.4	71.7	4.4	0.8	7.0	0.0
$4b_2$	19.73		0.0	22.8	0.2	29.5	33.9	0.7	12.6	0.4
$6a_1$	18.97	18.6	4.0	3.5	0.0	39.3	31.2	0.9	20.3	0.8
$7a_1$	18.3	17.357	2.2	20.5	0.3	6.2	45.8	0.4	24.3	0.4
$1b_1$	15.15	15.08	0.0	62.9	0.3	0.0	34.1	2.4	0.0	0.2
$6b_2$	14.22	14.42	0.0	0.2	0.0	1.5	63.6	2.0	32.1	0.4
$8a_1$	14.02	13.75	1.5	32.9	0.0	0.0	42.8	2.3	20.4	0.2
$9a_1$	13.30	~13.0	2.1	18.3	0.1	0.1	66.7	2.2	9.8	0.7
$2b_1$	10.28	10.320	0.0	21.6	0.0	0.0	73.5	4.1	0.0	0.8
$1a_2$	8.82	8.900	0.0	0.0	0.5	0.0	95.2	2.9	0.0	1.3

Results and Discussion

Threshold Photoelectron Spectrum. The valence shell threshold photoelectron spectrum of THF is plotted in Figure 1a, together with the OVGF ionization energies and relative spectral intensities. The corresponding data for furan[38] are also shown, to facilitate a comparison between these closely related molecules. In both molecules the predicted ionization energies for the outer valence orbitals agree reasonably well with the observed values, thereby enabling structure in the experimental spectra to be correlated with ionization from specific molecular orbitals. The experimental vertical ionization energies of THF, obtained through inspection of the threshold photoelectron spectrum, are listed in Table 1. The OVGF calculations demonstrate that the molecular orbital model of ionization[39] holds for the thirteen least tightly bound orbitals. The charge distributions listed for the OVGF ionization energies of Table 1 were calculated from the single-determinant HF wave function. Although these values do not explicitly account for the multireference nature of the OVGF method, for example, through the Dyson orbital populations, the calculated pole strengths (all >0.90) for the valence orbitals suggest that the one-particle picture holds quite well from the ionization threshold up to and including the 5b ionization. With each ionization dominated by the associated single-particle HF orbital (the principal molecular orbital for the ionization in question) the HF charge distribution should provide a qualitative account of the ionization process.

The He I excited photoelectron spectrum[40−47] and the Penning ionization spectrum[40,48] of THF have been recorded previously and many of the features in those spectra have corresponding structure in the threshold photoelectron spectrum (Figure 1a). However, the signal in a conventional He I excited electron energy resolved spectrum arises predominantly through direct photoionization. In contrast, resonant autoionization, an indirect two-step process, often influences threshold photoelectron spectra and can affect both the band profile and the relative intensity. Experimentally, it has been found that the relative intensities of photoelectron bands associated with weakly bound orbitals tend to be greater in conventional spectra than those in threshold photoelectron spectra, whereas the converse holds for the more tightly bound orbitals.[38,49] The enhancement in the latter bands can be attributed to resonant autoionization from numerous superexcited (Rydberg or valence) states. The OVGF pole strengths correspond to the relative intensities for direct transitions between the initial neutral ground state and the final ionic states. Indirect processes, such as autoionization, are not taken into account. As the signal in a threshold photoelectron spectrum can be influenced by resonant autoionization, the calculated pole strengths plotted in Figure 1 may not correspond quantitatively with the measured band intensities.

According to the OVGF calculations, the ionization energy of the outermost 9b orbital is ~1.6 eV lower than that of the next (11a) orbital. These theoretical predictions correlate satisfactorily with the experimental spectrum, which exhibits a

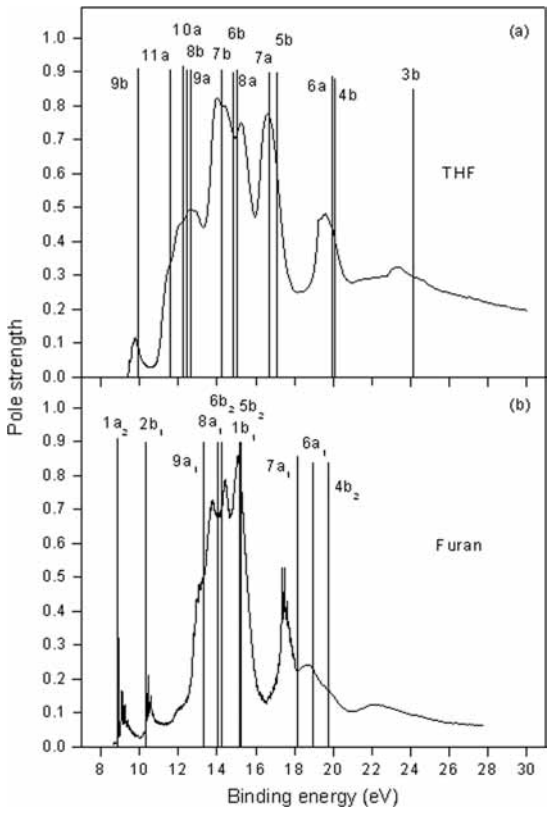

Figure 1. (a) Threshold photoelectron spectrum of THF together with the theoretical results (Table 1). The height of the bar is proportional to the calculated relative spectral intensity (pole strength). (b) Threshold photoelectron spectrum of furan together with the theoretical results (Table 2). The height of the bar is proportional to the calculated relative spectral intensity (pole strength).

well separated band, having a vertical ionization energy of 9.76 eV, associated with the 9b orbital, and a shoulder in the next band at 11.41 eV, related to the 11a orbital. The next three orbitals (10a, 8b, and 9a) have similar binding energies and ionization results in overlapping bands with maxima at 11.96, 12.59, and 12.84 eV. The calculated (14.23 eV) and observed (13.99 eV) ionization energies for the 7b orbital are in satisfactory agreement and correspond with the most intense feature in the threshold photoelectron spectrum (Figure 1a). Distinct maxima can be associated with the next two (6b and 8a) orbitals, although the calculated energies (14.86 and 15.02 eV) lie too close together. The OVGF ionization energies of the 7a and 5b orbitals are similar (Table 1) and give rise to a single peak in the threshold photoelectron spectrum. The same situation applies to ionization from the 6a and 4b orbitals, resulting in the band observed at 19.6 eV.

For the inner valence 3b, 5a, and 4a orbitals, configuration interaction results in the intensity associated with a particular orbital being redistributed among numerous satellite states. Under these circumstances, main lines may no longer be distinguishable. Probably the 3b orbital, and possibly the 5a orbital, are associated with the broad doublet appearing at 23.3 and 24.5 eV, but the strong continuum observed in this energy region demonstrates that most of the intensity is due to a multitude of overlapping satellite states. It is noticeable that the threshold photoelectron yield remains finite across the entire excitation range, including the Franck−Condon gap between the $(9b)^{-1}$ $\tilde{X}$ ^2B and the $(11a)^{-1}$ $\tilde{A}$ ^2A states, where the intensity drops significantly in the HeI excited spectrum.

Vibrational structure is observed only in the $(9b)^{-1}$ $\tilde{X}$ ^2B state threshold photoelectron band of THF, and Figure 2 shows this

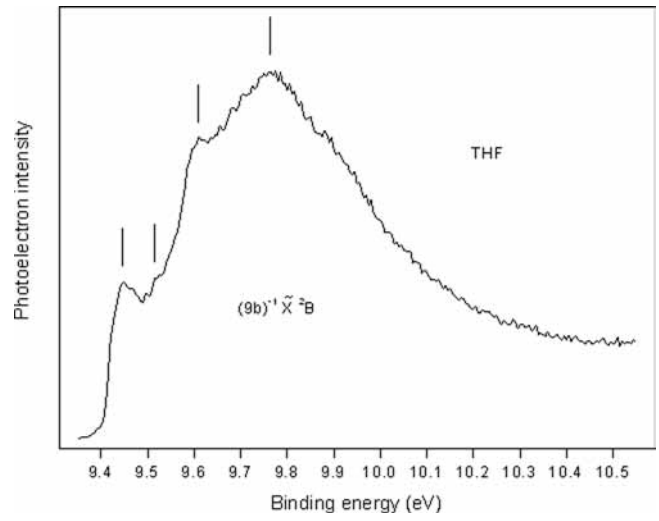

Figure 2. The $\tilde{X}$ ^2B state threshold photoelectron spectrum of THF. The vertical lines denote vibrational details.

band in greater detail. Far more extensive vibrational structure occurs in the spectrum of furan (Figure 1b) where excitation from the $1a_2$, $2b_1$, $9a_1$, and $7a_1$ orbitals gives rise to extended progressions.[38] Previous results for the ionization energy of the 9a orbital in THF differ considerably, in part because it is not always evident whether the published value refers to the adiabatic or to the vertical ionization energy. The present threshold photoelectron spectrum (Figure 2) indicates that the adiabatic and vertical ionization energies are separated by more than 0.3 eV. However, the corresponding vibrational structure was rarely observed in the He I excited photoelectron spectra due to insufficient resolution. From inspection of the present spectrum, we obtain adiabatic and vertical ionization energies for the 9b orbital of 9.445 ± 0.010 and 9.762 ± 0.010 eV, respectively. Our value for the adiabatic ionization energy agrees satisfactorily with that of 9.42 eV given by Hernandez[50] from an extrapolation of Rydberg series.

The assignment of the vibrational structure in the $\tilde{X}$ ^2B state threshold photoelectron band presents difficulties. First, the width of the peaks indicates that more than one mode is implicated, and second, several of the likely modes fall into groups having similar energies.[51] As an initial step toward assigning the $\tilde{X}$ ^2B state vibrational structure, we consider complementary information obtained in photoabsorption and electron impact studies. The photoabsorption spectrum of THF has been measured between 5.5 and 10.8 eV, and several bands associated with Rydberg series converging onto the $\tilde{X}$ ^2B ionization limit have been observed.[50,52−55] Some of these absorption bands exhibit weak vibrational progressions, but only the ring puckering mode, which has a vibrational energy of ∼30 meV,[53] has been identified. More extensive vibrational excitation in THF, involving several modes, has been observed in three studies employing electron impact.[56−58] The results from these experimental investigations are consistent with each other and, according to Allan,[56] the principal excitations, in terms of vibrational energies and modes, may be described as follows: 86 meV, ring-bend vibration ν_{16}; a group of C−C stretch and CH_2 rock vibrations, of which the asymmetric C−C stretch ν_{14} (109 meV) and ν_{13} (114 meV) appear dominant; ∼180 meV, associated with a group of vibrations with CH_2 scissoring character, particularly ν_6 (183 meV) and ν_5 (187 meV); ∼363 meV, a group of C−H stretch vibrations.

In the $\tilde{X}$ ^2B state threshold photoelectron spectrum (Figure 2) vibrational structure appears at energy intervals of 70, 163,

and 317 meV above the peak attributed to the adiabatic transition. On the basis of the evidence obtained from the electron impact studies,[56−58] we tentatively propose the following assignments. The shoulder at 9.515 eV could be ascribed to the ν_{16}^+ mode, and the peak at 9.608 eV could be due to either the ν_5^+ or ν_6^+ modes. The broad maximum at 9.762 eV could be associated with a single quantum of one of the C−H stretch vibrations or possibly two quanta of the ν_5^+ or ν_6^+ modes. However, as already mentioned, the width of the bands suggests that several vibrational modes are involved. Some of the vibrational excitation may be due to resonant autoionization from superexcited states as this two-step process is known to enhance vibrational populations in modes that may not be excited significantly in direct photoionization.

The bonding properties of the molecular orbitals in THF may be characterized by using the charge distribution analysis listed in Table 1, together with the results derived by Yamauchi et al.[40] The outermost 9b orbital, which lies perpendicular to the molecular plane, has the majority of its electron distribution associated with the oxygen atom. However, it should not be considered simply as an oxygen nonbonding atomic orbital, as is the case for the outermost $1a_2$ orbital in furan (Table 2). According to Yamauchi et al.,[40] the 11a and 9a orbitals are of similar type and may be characterized as $n_{O||},\sigma_{CC}$ and $n_{O||},\sigma_{CH}$, respectively, while the 10a and 8b orbitals, also of similar type, may be characterized as σ_{CH} and σ_{CH},σ_{CC}, respectively. These characterizations are consistent with the present charge distribution analyses. Tables 1 and 2 show that many of the orbitals in furan have corresponding orbitals in THF with very similar atomic populations. For example, the $9a_1$, $8a_1$, $6b_2$, and $5b_2$ orbitals in furan clearly correlate with the 11a, 9a, 8b, and 7b orbitals in THF. The next orbital in furan, $1b_1(\pi)$, is due to a bonding combination of p-orbitals on all the ring atoms, with a significant contribution from the oxygen atom. This molecular orbital is modified significantly in THF. However, the more tightly bound $7a_1$, $6a_1$, $4b_2$, $3b_2$, and $5a_1$ orbitals in furan evidently correlate with the 7a, 6a, 4b, 3b, and 5a orbitals in THF.

Ion Structures. The optimized geometries for all of the ions discussed in this study are shown in Figure 3 along with selected geometrical parameters. Gaussian 98 archive entries are available as Supporting Information. Relative energies are reported in Table 3.

THF Neutral, Ion, and Distonic Isomer. Both the THF neutral and ion optmized to C_2 symmetry structures. The geometrical parameters are quite similar for the two species (Figure 3). The most notable differences are the shortening of the C−O bond from 1.4337 to 1.429 Å, and the elongation of the symmetry unique C−C bond from 1.537 to 1.545 Å upon ionization. Removal of a p-orbital electron from the oxygen atom makes it effectively neutral (from having a significant negative charge in the neutral molecule). The charge on the adjacent methylene groups doubles from +0.19 to +0.38, while that on the remaining methylene groups increases from essentially zero to +0.12. The increase in charge density on the C−O−C part of the skeleton is consistent with virtually all of the spin density being spread across this moiety in the ion. The spin density can contribute to partial π-bonding, which will decrease the C−O bond length in the ion. The increase in charge density on the two remaining methylene groups, along with an absence of spin density, leads to an increased C−C bond upon ionization. The distonic isomer $^{\bullet}CH_2CH_2CH_2OCH_2^+$ has its spin density entirely on the terminal CH_2 group of the propyl chain. Charge density is not localized on the expected CH_2 group but rather

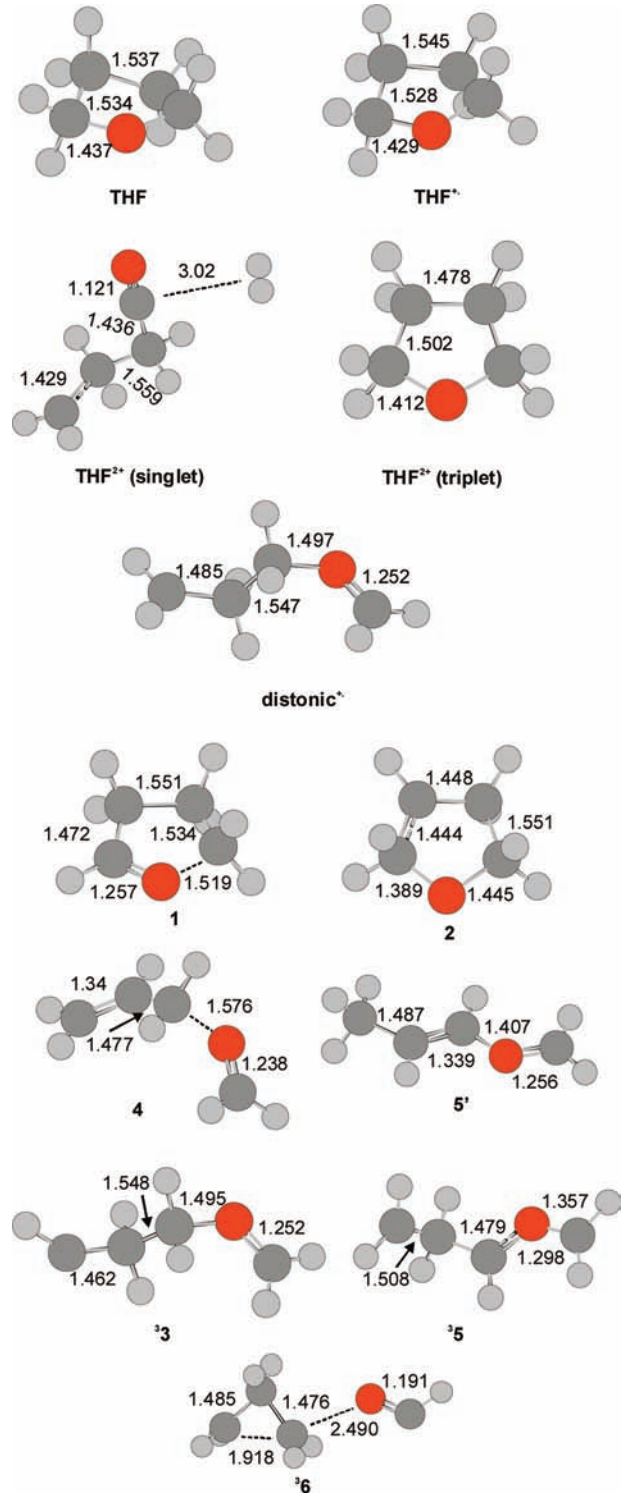

Figure 3. B3-LYP/6-31+G(d) optimized structures for the ions investigated in this work. Bond lengths in Å.

split between it (+0.56) and the propyl chain (+0.44). A C−O bond length of 1.252 Å clearly indicates that double bond formation is involved in delocalizing the charge from this CH_2 group.

THF Dications. The triplet THF dication optimized to a C_{2v} symmetry structure (Figure 3). The charge is essentially divided between the methylene groups, with the oxygen atom being neutral. The C−O and C−C bond lengths are universally shortened in the dication relative to the monocation. This is consistent with the increase in spin density at all CH_2 groups

TABLE 3: Comparison of Experimental and Calculated Relative Energies (kJ mol^{-1}) at 0 K

ion	B3-LYP/6-31+G(d)	G3	experiment[a]
THF	−878.8	−914.9 (−9.48 eV)	−906.9
$THF^{+\bullet}$	0	0	0
$THF^{2+\bullet\bullet}$ (triplet)	1556.6	1608.4 (16.7 eV)	
THF^{2+} (singlet)[b]	1363.5	1321.3 (13.7 eV)	
$^{\bullet}CH_2CH_2CH_2OCH_2^+$	82.4	70.1	
1 + H	100.1	71.7,[c] 73.5[d]	78 ±1,[c,e]82±3,[c,f]80.5[g]
2 + H	251.4		
^{1}**4** + H	232.5		
^{1}**5′** + H	210.4		
^{3}**3** + H	535.3		
^{3}**5** + H	434.0		
^{3}**6** + H	482.5		

[a] Literature values have been corrected to 0 K when necessary. [b] Unoptimized structure, but predicted change in energy less than 10^{-3} kJ mol^{-1} for 37 iterations. All frequencies positive. [c] Present work. [d] Employing $\Delta_f H°_{298}$ of 591 kJ mol^{-1} for **1**, $\Delta_f H°_{298}$ of −184 kJ mol^{-1} for THF reported by Kabli et al.[12] and the G3 IE of 9.48 eV. [e] Employing the G3 IE of 9.48 eV to correct photon energy to internal energy. [f] Employing the experimental IE of 9.445 ± 0.010 eV to correct photon energy to internal energy. [g] Employing the measured proton affinity of 2,3-dihydrofuran reported by Bouchoux and co-workers[10] (870 kJ mol^{-1}) and the dihydrofuran $\Delta_f H°_{298}$ of −72.25 ± 0.41 kJ mol^{-1} reported by NIST[21] (see text).

in the dication, resulting in significant partial π-bonding. This is especially true for the methylene groups in the 3 and 4 positions in the ring, which take on almost an entire unpaired spin. The presence of partial π-bonding is also supported by the change in symmetry from C_2 in the THF monocation to C_{2v} in the dication. We were unable to fully optimize the singlet dication, though the structure shown in Figure 3 was the final structure after 37 optimization iterations during which the predicted change in energy was less than 10^{-3} kJ mol^{-1}. It is a ring-opened structure in which a dication interacts with a neutral molecule of H_2. The dication portion of the structure is a vinyl-protonated acylium ion, with positive charge located primarily on the carbonyl carbon (formal charge of + 0.86) and the terminal methylene group (+0.82). The geometry of the CH_2CH_2 group has the appearance of a distorted planar vinyl group interacting with a hydrogen atom.

Fragment Ions. Loss of a hydrogen atom from the 2 or 3 position of the THF monocation results in fragment ions **1** and **2**, respectively (Figure 3). Ion **1** has what is essentially a double bond between the CH and O groups, and the charge is largely split between the CH group (+0.60) and the CH_2 group on the other side of the O atom (+0.30). The charge in **2** is spread across the CH_2CHCH_2 moiety, and the bond lengths are consistent with an allyl-like geometry. The puckering of the ring so evident in the THF neutral and monocation is now greatly diminished in these two fragment ions, due principally to the increase in delocalization of the charge, and hence partial π-bonding.

Hydrogen atom loss from the distonic isomer was explored by removing one from each of the four carbon atoms to generate both singlet and triplet state cations: $CHCH_2CH_2OCH_2$ (**3**), $CH_2CHCH_2OCH_2$ (**4**), $CH_2CH_2CHOCH_2$ (**5**), and $CH_2CH_2CH_2OCH$ (**6**). For singlet species, we were unable to get the calculations to converge for ion **3**. Ion **4** is a propenyl-substituted $-OCH_2^+$ cation. The CH_2CHCH_2 group is planar, indicating delocalization of +0.41 charge (but not completely as the bond lengths are not the same). This group interacts with a formaldehyde molecule that shares +0.59 charge. Attempts to find an equilibrium structure for singlet state **5** resulted in 1,2-H atom transfer to form **5′**, $CH_3CH{=}CHOCH_2^+$. Attempts to find an equilibrium structure for singlet state **6** resulted in 1,4-H-atom transfer to form **4**. Ions **3**, **5**, and **6** do correspond to equilibrium structures on the triplet state surface (Figure 3), but these are all significantly higher in energy than their singlet state counterparts (Table 3). Triplet state **3** (^{3}**3**) has both spins on the terminal carbene carbon and the charge is split between the OCH_2 group (+0.54) and the rest of the ion (+0.46). Triplet state **5** (^{3}**5**) has a planar CH_2OCH group consistent with delocalization of the spin (+1) and charge (+0.83) across this moiety. The remaining spin is localized on the terminal methylene group. This group sits up out of the plain of the CH_2OCH group, allowing its singly occupied π-orbital to interact with the π-cloud of the latter. Triplet state **6** (^{3}**6**) is essentially a neutral formyl radical (spin +1) interacting with a cyclopropane/trimethylene[59] cation (charge +1, spin +1).

Threshold Photoelectron Photoion Coincidence Spectroscopy. Coincidence spectra were collected in the photon energy range 9.9−34 eV. Breakdown curves for all observed ions are presented in Figure 4, and appearance energies (AEs) of the fragment ions, derived from the TOF spectra, are listed along with literature values in Table 4. The large uncertainty quoted with our AE is due solely to the energy spacing at which the TOF spectra were measured. The lowest energy dissociation is the expected H loss to form *m/z* 71. The ions appear at the lowest measured photon energy of 9.90 ± 0.05 eV, which is lower than the earlier electron ionization AE measured by Collin and Conde-Caprace[60] (10.44 eV) due both to smearing out of our breakdown diagrams near the dissociation threshold from experimental parameters, in particular the electron transmission function, and their use of electrons with a poor energy resolution. Gallegos and Kiser[61] also employed low energy-resolution electrons in their AE measurements, and as expected the presently measured thresholds are all lower than the previously reported values.

The loss of a hydrogen atom occurs over the photon energy range 9.9−10.4 eV. The photon energy was converted to internal energy of the THF ion using our presently measured adiabatic ionization energy, IE_a, value of 9.445 ± 0.010 eV, which lies between the reported value of 9.40 ± 0.02 eV[21] and the G3 value of 9.48 eV. The results for the three ion source residence times, along with a representative fit to the data are presented in Figure 5. There is a small but non-negligible kinetic shift in the data, necessitating kinetic modeling of the data (Figure 5a). The fitting yields an E_0 of 0.85 ± 0.03 eV (82 ± 3 kJ mol^{-1}). This corresponds to an AE of 10.30 ± 0.04 eV. If the G3 IE of 9.48 eV is used to convert the data, E_0 = 0.81 ± 0.01 eV (78 ± 1 kJ mol^{-1}), not including the estimated maximum error in the G3 IE of ±0.08 eV.[20] The latter value is closer to the G3

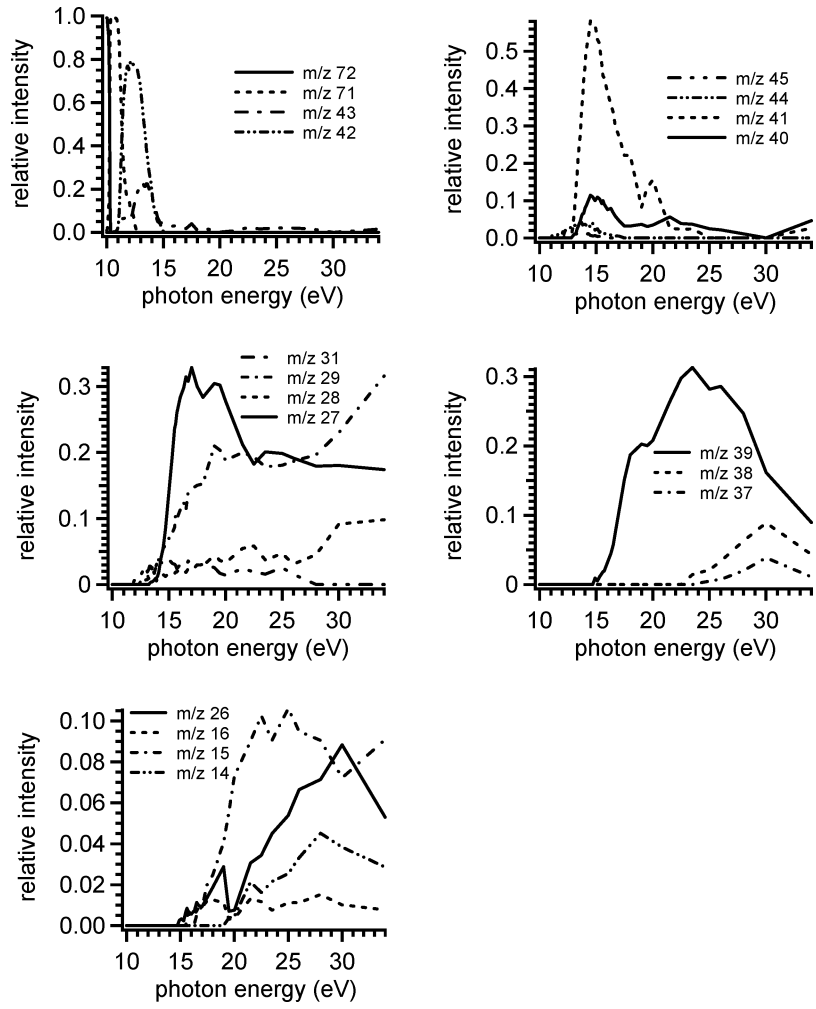

Figure 4. Breakdown curves for all observed fragment ions from ionized THF at an ion source residence time of 1.116 μs.

TABLE 4: Fragment Ion Appearance Energies (eV) at 298 K for THF

m/z	this work	Gallegos and Kiser[61]	Collin and Conde-Caprace[60]
71	$<10.0 \pm 0.1$[a]	11.1 ± 0.2	10.44
45	12.15 ± 0.10		
44	11.0 ± 0.1		12.27
43	10.9 ± 0.2	12.8 ± 0.2	11.87
42	10.65 ± 0.20	12.7 ± 0.2	11.54
41	12.7 ± 0.2	15.5 ± 0.3	13.72
40	12.9 ± 0.1	15.2 ± 0.3	
39	14.9 ± 0.2	18.7 ± 0.6	
38	23.5 ± 0.2		
37	25 ± 1		
31	11.85 ± 0.10		
29	12.5 ± 0.2	15.8 ± 0.2	
28	12.5 ± 0.2		
27	13.3 ± 0.1	16.1 ± 0.3	
26	14.9 ± 0.2	17.3 ± 0.3	
16	15.6 ± 0.1		
15	16.0 ± 0.3		
14	19.5 ± 0.5		

[a] This value is greatly affected by experimental smearing of the breakdown curves near the ionization threshold.

E_0 of 72 kJ mol^{-1} for the formation of ion **1**. A variety of ring-opening reactions were also probed at the B3-LYP/6-31+G(d) level of theory (Table 3). The distonic isomer $^{\bullet}CH_2CH_2CH_2OCH_2^+$ lies 70 kJ mol^{-1} higher than ionized THF, which places it within 1 kJ mol^{-1} of the threshold for the dissociation to **1** (without taking into account the transition state for the interconversion). All of the probed H-loss products from the distonic isomer (which includes singlet and triplet species, Table 3) lie significantly higher in energy than ion **1**, eliminating the possibility that ionized THF dissociates to *m/z* 71 via a ring-opening reaction in the present experiment.

The entropy of activation, $\Delta^{\ddagger}S$, values for the two fits fall in a similar range, 8 ± 5 J K^{-1} mol^{-1}. This value is also consistent with the formation of **1**. The ΔS for this channel is 107 J K^{-1} mol^{-1} ($\Delta S_{vib,rot} = -1.7$ and $\Delta S_{trans} = 108.6$ J K^{-1} mol^{-1}, from statistical mechanics calculations). Typically, the dividing surface corresponding to the H-loss variational transition state lies close in geometry to that of the reacting ion, and so $\Delta^{\ddagger}S$ should lie close to $\Delta S_{vib,rot}$, ~ 0 J K^{-1} mol^{-1}.[35,36] On the other hand, if ionized THF ring opens during the dissociation, a large gain in entropy will result. For example, if we assume the barrier to the isomerization of ionized THF to the distonic isomer is small, the potential energy surface for the dissociation to product ions **3**−**6** can be approximated with a single potential energy well. This variational transition state should resemble the distonic isomer. The ΔS for the conversion of ionized THF to $^{\bullet}CH_2CH_2CH_2OCH_2^+$ is 41 J K^{-1} mol^{-1}, while the ΔS for the conversion of ionized THF to the **3** + H (as an example) is 129 J K^{-1} mol^{-1} ($\Delta S_{vib,rot} = 20.8$ and $\Delta S_{trans} = 108.6$ J K^{-1} mol^{-1}), and thus $\Delta^{\ddagger}S$ could be expected to be between 20 and 40 J K^{-1} mol^{-1}. So, there does not seem to be evidence for the formation of noncyclic *m/z* 71 ion in the decomposition of ionized THF. Moreover, van Houte and van Thuijl,[13] whose

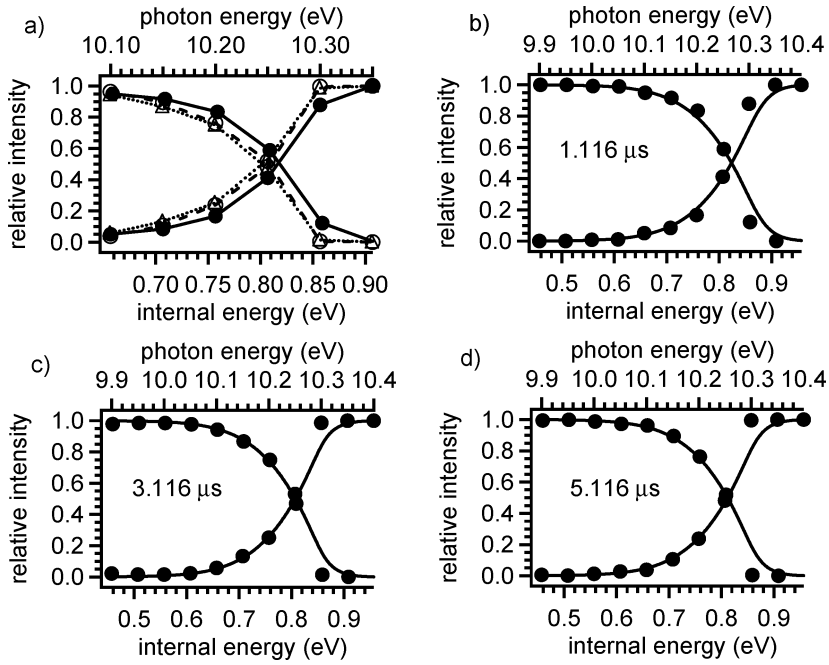

Figure 5. Threshold breakdown curves for H loss at three ion source residence times. (a) Experimental data at 1.116 ms (●), 3.116 ms (○), and 5.116 ms (Δ). Data are connected with straight lines. (b)−(d) Representative fit to the experimental data in (a). Experimental data are the solid points and the theoretical fits are solid lines.

TABLE 5: Comparison of Experimental and Calculated $\Delta_f H°$ Values (kJ mol^{-1})

	G3		experiment[a]	
ion	0 K	298 K	0 K	298 K
THF	−149.5	−178.6	−154.5	−184.2
$THF^{+\bullet}$	765.4	735.9	752, 756.2 ± 2[e]	722.7
$^{\bullet}CH_2CH_2CH_2OCH_2^+$	835.5	811.3		
1	621.1,[b] 616.6[c]	595.4,[b] 591[c]	620 ± 4[b]	594 ± 4,[b] 588[d]

[a] Literature values are those reported by NIST,[21] unless otherwise specified. Values have been temperature corrected when necessary. [b] Present work. [c] Kabli et al.[12] [d] Employing the measured proton affinity of 2,3-dihydrofuran reported by Bouchoux and co-workers[10] (870 kJ mol^{-1}) and the dihydrofuran $\Delta_f H°_{298}$ of −72.25 ± 0.41 kJ mol^{-1} reported by NIST[21] (see text). [e] See text.

collision cross section measurements were consistent with noncyclic species, generated their ions by electron ionization (employing both 20 and 70 eV electrons) in the ion source of a mass spectrometer. The collision cell was located in the first field-free region of the instrument, which means that the colliding ions would have a wide range of internal energies. At higher internal energies than those explored in this TPEPICO study, it might be expected that the ring-opening reaction leading to the distonic ion and its noncyclic fragmentation products would start to out-compete formation of **1** due to more favorable entropy effects.

Thermochemistry. The experimentally derived E_0 values can be used to derive the $\Delta_f H°_0$ for ion **1**. Together with the $\Delta_f H°_0$ values for the THF ion (756.4 ± 2 kJ mol^{-1}, derived from the neutral $\Delta_f H°_0$ of -154.9 ± 0.7 kJ mol^{-1},[21] and experimental IE of 9.445 ± 0.010 eV) and H atom (218.5 kJ mol^{-1})[21] our E_0 of 82 ± 3 kJ mol^{-1} yields a $\Delta_f H°_0$ for ion **1** of 620 ± 4 kJ mol^{-1} ($\Delta_f H°_{298}$ = 594 ± 4 kJ mol^{-1}), in good agreement with the G3 $\Delta_f H°_0$ of 621 (Table 5). If the G3 IE of 9.48 eV is used, along with our corresponding E_0 of 78 ± 1 kJ mol^{-1}, the $\Delta_f H°_0$ for ion **1** remains 619 ± 1 kJ mol^{-1} ($\Delta_f H°_{298}$ = 593 ± 1 kJ mol^{-1}), the difference in E_0 being due to the discrepancy in the two IE values used to correct the data. Bouchoux and co-workers[10] determined the $\Delta_f H°_{298}$ of **1** to be 545 kJ mol^{-1} based on a measured proton affinity value for dihydrofuran of 870 kJ mol^{-1} and an estimated 2,3-dihydrofuran $\Delta_f H°_{298}$ of −115 kJ mol^{-1}. If the $\Delta_f H°_{298}$ for 2,3-dihydrofuran of −72.25 ± 0.41 kJ mol^{-1} reported by NIST[21] is used, $\Delta_f H°_{298}$ **1** = 588 kJ mol^{-1}, which is closer to the present estimate.

Charge Separation Reactions in Doubly Ionized THF Cations. Ion TOF spectra recorded at photon energies of 21.5 and 30 eV are shown in Figure 6, and it is noticeable that the widths of some of the peaks, particularly those associated with *m/z* 15, 29, or 39 are broader in the spectrum recorded at 30 eV than in that recorded at 21.5 eV. For example, the fwhm of the *m/z* 29 peak recorded at 30 eV is a factor of 3 larger than that recorded at 21.5 eV. The peak width is dependent upon the fragment ion initial kinetic energy and can be used to deduce the double ionization threshold in molecules where the doubly charged parent ion is unstable in relation to the time scale relevant to the measurement (microseconds in the present experiment). In furan the doubly charged parent ion was observed and a threshold of 25.50 eV was determined,[38] in good agreement with calculated energies of 25.15 and 25.16 eV for the singlet and triplet states, respectively, of doubly ionized furan. In THF, the corresponding theoretical energies for the singlet and triplet states are 23.18 and 26.18 eV, respectively (Table 3). However, the doubly charged parent ion was not observed in the present experiment, thereby indicating that a rapid fragmentation takes place to produce two singly charged species. The TOF spectra (Figure 6) suggest that the initially created doubly charged parent ion probably fragments to form *m/z* 15, together with *m/z* 29 or 39, plus a neutral species. Other fragmentations are also possible. Our previous work[62] has shown

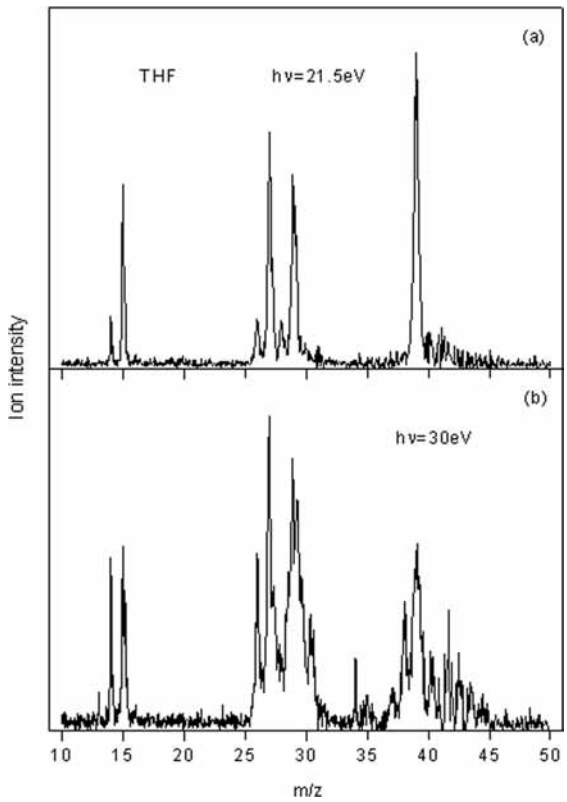

Figure 6. Ion TOF spectra of THF recorded at photon energies of (a) 21.5 eV and (b) 30 eV.

that the width of the *m*/*z* 15 peak provides a reliable indication of the double ionization threshold in molecules where the doubly charged parent ion is not observed experimentally because it appears that this fragment is often formed in combination with another small fragment ion in the dissociation of the doubly charged parent ion. However, in THF the broadening is most apparent in the *m*/*z* 29 peak. Fragment peak broadening becomes evident at excitation energies of 25 eV, and above, thereby placing an upper limit on the double ionization energy. Thus, the experimental value falls between those calculated for the singlet and triplet states.

Conclusions

The threshold photoelectron spectrum of tetrahydrofuran (THF) is compared to that of its unsaturated analogue, furan. There is a general similarity in the orbital assignments between the two molecules, although furan exhibits greater vibrational details. An adiabatic ionization energy of 9.445 ± 0.010 eV has been derived from the onset of the TPES spectrum. RRKM fitting of the threshold photoelectron photoion coincidence spectroscopy breakdown curves for the loss of a hydrogen atom from ionized THF over the photon energy range 9.9−10.4 eV yielded an E_0 of 0.85 ± 0.03 eV (82 ± 3 kJ mol^{-1}). If the G3 IE of 9.48 eV was used to convert the experimental data from photon energy to THF ion internal energy, a value of $E_0 = 0.81$ ± 0.01 eV (78 ± 1 kJ mol^{-1}) was found. The latter value is closer to the G3 E_0 of 72 kJ mol^{-1} for the formation of the cyclic ion **1**. Ring-opening reactions involving the distonic isomer $^{\bullet}CH_2CH_2CH_2OCH_2^+$ were also probed at the B3-LYP/6-31+G(d) and G3 levels of theory and all lie significantly higher in energy than ion **1**, eliminating the possibility that ionized THF dissociates to *m*/*z* 71 via a ring-opening reaction in the present experiment. The experimentally derived E_0 values were used to derive a $\Delta_f H^o_0$ for ion **1**, 620 ± 4 kJ mol^{-1} ($\Delta_f H^o_{298}$ = 594 ± 4 kJ mol^{-1}), in good agreement with the G3 $\Delta_f H^o_0$ of 621 kJ mol^{-1}.

Acknowledgment. We are grateful to the Council for the Central Laboratory of the Research Councils (U.K.) for the allocation of beam time at the Daresbury Laboratory Synchrotron Radiation Source. P.M.M. thanks the Natural Sciences and Engineering Research Council of Canada for continuing financial support and the University of Ottawa for seed funds to undertake these experiments.

Supporting Information Available: Gaussian archive entries for all species explored in this study. This material is available free of charge via the Internet at http://pubs.acs.org.

References and Notes

(1) Krenmayr, P. *Monatsh. Chem.* **1975**, *106*, 925.
(2) Wright, A. D.; Bowen, R. D. *Can. J. Chem.* **1993**, *71*, 1073.
(3) Stolze, R.; Budzikiewicz, H. *Tetrahedron* **1981**, *37*, 781.
(4) Bowen, R. D. *J. Chem. Soc., Chem. Commun.* **1985**, 807.
(5) Bowen, R. D.; Wright, A. D.; Derrick, P. J. *J. Chem. Soc., Perkin Trans. 2* **1993**, 501.
(6) Hegedüs Vajda, J.; Harrison, A. G. *Int. J. Mass Spectrom. Ion Phys.* **1979**, *30*, 293.
(7) Bowen, R. D.; Colburn, A. W.; Derrick, P. J. *Org. Mass Spectrom.* **1992**, *27*, 625.
(8) Milliet, A.; Sozzi, G.; Audier, H. E. *Org. Mass Spectrom.* **1992**, *27*, 787.
(9) Bouchoux, G.; Hoppiiliard, Y.; Jaudon, P. *Org. Mass Spectrom.* **1987**, *22*, 98.
(10) Bouchoux, G.; Djazi, F.; Hoppilliard, Y.; Houriet, R.; Rolli, E. *Org. Mass Spectrom.* **1986**, *21*, 209.
(11) Laderoute, K. R.; Zwinselman, J. J.; Harrison, A. G. *Org. Mass Spectrom.* **1985**, *20*, 25.
(12) Kabli, S.; van Beelen, E. S. E.; Ingemann, S.; Henriksen, L.; Hammerum, S. *Int. J. Mass Spectrom.* **2006**, *249*−*250*, 370.
(13) van Houte, J. J.; van Thuijl, J. *Int. J. Mass Spectrom. Ion Process.* **1994**, *133*, 121.
(14) Holland, D. M. P.; Shaw, D. A.; Sumner, I.; Hayes, M. A.; Mackie, R. A.; Wannberg, B.; Shpinkova, L. G.; Rennie, E. E.; Cooper, L.; Johnson, C. A. F.; Parker, J. E. *Nucl. Instrum. Meth. B* **2001**, *179*, 436.
(15) Holland, D. M. P.; West, J. B.; MacDowell, A. A.; Munro, I. H.; Beckett, A. G. *Nucl. Instrum. Methods* **1989**, *B44*, 233.
(16) Stockbauer, R. *Int. J. Mass Spectrom. Ion Phys.* **1977**, *25*, 89.
(17) Hehre, W. J.; Radom, L.; Schleyer, P. v. R.; Pople, J. A. *Ab Initio Molecular Orbital Theory*; Wiley: New York, 1986.
(18) Frisch, M. J.; Trucks, G. W.; Schlegel, H. B.; Scuseria, G. E.; Robb, M. A.; Cheeseman, J. R.; Zakrzewski, V. G.; Montgomery, J. A.; Stratmann, R. E.; Burant, J. C.; Dapprich, S.; Millam, J. M.; Daniels, A. D.; Kudin, K. N.; Strain, M. C.; Farkas, O.; Tomasi, J.; Barone, V.; Cossi, M.; Cammi, R.; Mennucci, B.; Pomelli, C.; Adamo, C.; Clifford, S.; Ochterski, J.; Petersson, G. A.; Ayala, P. Y.; Cui, Q.; Morokuma, K.; Malick, D. K.; Rabuck, A. D.; Raghavachari, K.; Foresman, J. B.; Cioslowski, J.; Ortiz, J. V.; Stefanov, B. B.; Liu, G.; Liashenko, A.; Piskorz, P.; Komaromi, I.; Gomperts, R.; Martin, R. L.; Fox, D. J.; Keith, T.; Al-Laham, M. A.; Peng, C. Y.; Nanayakkara, A.; Gonzalez, C.; Challacombe, M.; Gill, P. M. W.; Johnson, B.; Chen, W.; Wong, M. W.; Andres, J. L.; Gonzalez, C.; Head-Gordon, M.; Replogle, E. S.; Pople, J. A., *Gaussian 98*, rev. A.6; Gaussian Inc.: Pittsburgh, PA, 1998.
(19) Scott, A. P.; Radom, L. *J. Phys. Chem.* **1996**, *100*, 16502.
(20) Curtiss, L. A.; Raghavachari, K.; Refern, P. C.; Rassolov, V.; Pople, J. A. *J. Chem. Phys.* **1998**, *109*, 7764.
(21) *NIST, Chemistry Webbook (NIST Standard Reference Database Number 69)*; National Institute of Standards and Technology: Gaithersburg, MD, 2005.
(22) Lias, S. G.; Bartmess, J. E.; Liebman, J. F.; Holmes, J. L.; Levin, R. D.; Mallard, W. G. *J. Phys. Chem. Ref. Data* **1988**, *17* (Suppl.1),
(23) Nicolaides, A.; Rauk, A.; Glukhovtsev, M. N.; Radom, L. *J. Phys. Chem.* **1996**, *100*, 17460.
(24) von Niessen, W.; Schirmer, J.; Cederbaum, L. S. *Comput. Phys. Rep.* **1984**, *1*, 57.
(25) Guest, M. F.; Lenthe, J. H. v.; Kendrick, J.; Schoffel, K.; Sherwood, P. *Users guide and reference manual, version 7, computing for science ltd.*; CCLRC Daresbury Laboratory: Daresbury, U.K., 2005.
(26) Guest, M. F.; Thomas, J. M. H.; Sherwood, P.; Bush, I. J.; Dam, H. J. J. v.; Lenthe, J. H. v.; Havenith, R. W. A.; Kendrick, J. *Mol. Phys.* **2005**, *103*, 719.

(27) Dunning, T. H. *J. Chem. Phys.* **1989**, *90*, 1007.
(28) Wilson, A. K.; Woon, D. E.; Peterson, K. A.; Dunning, T. H. *J. Chem. Phys.* **1999**, *110*, 7667.
(29) Woon, D. E.; Dunning, T. H. *J. Chem. Phys.* **1993**, *98*, 1358.
(30) Woon, D. E.; Dunning, T. H. *J. Chem. Phys.* **1994**, *100*, 2975.
(31) Baer, T.; Hase, W. L. *Unimolecular Reaction Dynamics, Theory and Experiments*; Oxford University Press: New York, 1996.
(32) Baer, T.; Mayer, P. M. *J. Am. Soc. Mass Spectrom.* **1997**, *8*, 103.
(33) Beyer, T.; Swinehart, D. R. *ACM Commun.* **1973**, *16*, 379.
(34) Rennie, E. E.; Boulanger, A.-M.; Mayer, P. M.; Holland, D. M. P.; Shaw, D. A.; Cooper, L.; Shpinkova, L. G. *J. Phys. Chem. A* **2006**, *110*, 8663.
(35) Boulanger, A. M.; Rennie, E. E.; Holland, D. M. P.; Shaw, D. A.; Mayer, P. M. *J. Phys. Chem. A* **2008**, *112*, 866.
(36) Boulanger, A.-M.; Rennie, E. E.; Holland, D. M. P.; Shaw, D. A.; Mayer, P. M. *J. Phys. Chem. A* **2007**, *111*, 5388.
(37) Rabaev, M.; Boulanger, A.-M.; Holland, D. M. P.; Shaw, D. A.; Mayer, P. M. *J. Phys. Chem. A* **2009**, *113*, 1518.
(38) Rennie, E. E.; Cooper, L.; Johnson, C. A. F.; Parker, J. E.; Mackie, R. A.; Shpinkova, L. G.; Holland, D. M. P.; Shaw, D. A.; Hayes, M. A. *Chem. Phys.* **2001**, *263*, 149.
(39) Cederbaum, L. S.; Domcke, W.; Schirmer, J.; Niessen, W. v. *Adv. Chem. Phys.* **1986**, *65*, 115.
(40) Yamauchi, M.; Yamakado, H.; Ohno, K. *J. Phys. Chem. A* **1997**, *101*, 6184.
(41) Tasaki, K.; Yang, X.; Urano, S.; Fetzer, S.; LeBreton, P. R. *J. Am. Chem. Soc.* **1990**, *112*, 538.
(42) Kimura, K.; Katsumata, S.; Achiba, Y.; Yamazaki, T.; Iwata, S. *Handbook of HeI Photoelectron Spectra of Fundamental Organic Molecules*; Japan Scientific Societies Press: Tokyo, 1979.
(43) Gerson, S. H.; Worley, S. D.; Nodor, N.; Kaminski, J. J.; Flechtner, T. W. *J. Electron Spectrosc. Relat. Phenom.* **1978**, *13*, 421.
(44) Behan, J. M.; Dean, F. M.; Johnstone, R. A. W. *Tetrahedron* **1976**, *32*, 167.
(45) Pignataro, S.; Distefano, G. *Chem. Phys. Lett.* **1974**, *26*, 356.
(46) Schmidt, H.; Schweig, A. *Chem. Ber.* **1974**, *107*, 725.
(47) Turner, D. W.; Baker, C.; Baker, A. D.; Brundle, C. R. *Molecular Photoelectron Spectroscopy*; Wiley: London, 1970.
(48) Yee, D. S. C.; Hamnett, A.; Brion, C. E. *J. Electron Spectrosc. Relat. Phenom.* **1976**, *8*, 291.
(49) Boulanger, A.-M.; Rennie, E. E.; Mayer, P. M.; Holland, D. M. P.; Shaw, D. A. *J. Phys. Chem. A* **2006**, *110*, 8563.
(50) Hernandez, G. J. *J. Chem. Phys.* **1963**, *38*, 2233.
(51) Cadioli, B.; Gallinella, E.; Coulombeau, C.; Jobic, H.; Berthier, G. *J. Phys. Chem.* **1993**, *97*, 7844.
(52) Bremner, L. J.; Curtis, M. G.; Walker, I. C. *J. Chem. Soc., Faraday Trans.* **1991**, *87*, 1049.
(53) Davidson, R.; Høg, J.; Warsop, P. A.; Whiteside, J. A. B. *Faraday Trans. II* **1972**, *68*, 1652.
(54) Doucet, J.; Sauvageau, P.; Sandorfy, C. *Chem. Phys. Lett.* **1972**, *17*, 316.
(55) Pickett, L. W.; Hoeflich, N. J.; Liu, T.-C. *J. Am. Chem. Soc.* **1951**, *73*, 4865.
(56) Allan, M. *J. Phys. B* **2007**, *40*, 3531.
(57) Milosavljević, A. R.; Giuliani, A.; Sević, D.; Hubin-Franskin, M.-J.; Marinković, B. P. *Eur. Phys. J.* **2005**, *D35*, 411.
(58) Lepage, M.; Letarte, S.; Michaud, M.; Motte-Tollet, F.; Hubin-Franskin, M.-J.; Roy, D.; Sanche, L. *J. Chem. Phys.* **1998**, *109*, 5980.
(59) Holmes, J. L.; Aubry, C.; Mayer, P. M. *Assigning Structures to Ions in Mass Spectrometry*; CRC Press: Boca Raton, FL, 2007.
(60) Collin, J. E.; Conde-Caprace, G. *Int. J. Mass Spectrom. Ion Phys.* **1968**, *1*, 213.
(61) Gallegos, E. J.; Kiser, R. W. *J. Phys. Chem.* **1962**, *66*, 136.
(62) Rennie, E. E.; Cooper, L.; Shpinkova, L. G.; Holland, D. M. P.; Shaw, D. A.; Guest, M. F.; Mayer, P. M. *J. Phys. Chem. A* **2009**, *113*, 5823.

JP906440P